SUPPORTING INFORMATION

Tackling the Activity and Selectivity Challenges of Electrocatalysts towards Nitrogen Reduction Reaction via Atomically Dispersed Bi-Atom Catalysts

Xiangyu Guo[†], Jinxing Gu[§], Shiru Lin[§], Shengli Zhang[‡,*], Zhongfang Chen[§,*], Shiping Huang[†,*]

[†] State Key Laboratory of Organic-Inorganic Composites, Beijing University of Chemical Technology, Beijing 100029, China

[§] Department of Chemistry, University of Puerto Rico, Rio Piedras, San Juan, PR 00931, USA

[‡] MIIT Key Laboratory of Advanced Display Materials and Devices, Ministry of Industry and Information Technology, Institute of Optoelectronics & Nanomaterials, Nanjing University of Science and Technology, Nanjing 210094, China

*Corresponding author E-mail:

zhangslvip@njust.edu.cn (SZ),

zhongfangchen@gmail.com (ZC),

huangsp@mail.buct.edu.cn (SH)

Gibbs Free Energy Computations

The Gibbs free energy (*G*) of the intermediates was calculated by using the computational hydrogen electrode (CHE) model proposed by Nørskov et al.[1] The chemical potential of the H^+/e^- pair in aqueous solution is related to that of half of the H_2 gas molecule at standard hydrogen electrode (SHE) conditions. According to this method, the *G* value can be determined as follows:

$$G = \Delta E - T\Delta S + \Delta ZPE + \Delta G_U + \Delta G_{pH}$$

Where ΔE is the reaction energy directly obtained from DFT calculations, and *T* is the temperature (T=298.15 K). *ΔZPE* and *ΔS* are the differences between the adsorbed species and the gas phase molecules in zero-point energy and entropy, respectively. ΔG_U is the free energy contribution related to applied potential *U*, which can be determined as $\Delta G_U = -eU$. The *U* value is determined by the equation $U = -\Delta G_{max}/e$, where ΔG_{max} is free energy change in potential-determining step. ΔG_{pH} is the correction of the free energy of H^+ ions by the concentration dependence of the entropy: $\Delta G_{pH} = 2.303 \times k_B \times pH$, where k_B is the Boltzmann constant, and the value of *pH* is set to be 0.

Thus, ΔG between two states involve in the N_2 reduction process can be expressed as to:

$$\Delta G = G(N_{2-m}H_n) + m\,G(NH_3) - G(N_2) - n/2\,G(H_2) - G(*)$$

where * denotes the surface of M_2-Pc, *n* is the number of H+/e- pairs transferred, and m (m=0, 1) is the number of NH_3 molecules released. For example, for n=m=0, the Gibbs free energy change leads to the N_2 adsorption variation:

$$\Delta G\,(N_2, \text{ads.}) = G(N_2*) - G(N_2) - G\,(*)$$

The zero-point energies and entropies of the reaction species were calculated from the vibrational frequencies. During these frequency calculations, all atoms of substrate were rigidly constrained so that no additional degrees of freedom, due to the catalyst, are introduced in to the reacting system. For gas

phase molecule, the entropy term can be expressed as the sum of the translational, rotational and vibrational contributions, whereas for adsorbates the translational and rotational entropy were not taken into account due to negligible contributions. The thermodynamic quantities for the N_2, H_2, NH_3 species in the gas phase are shown in **Table S9**.

Kinetic Computations

The transition states (TS) were identified using the climbing image nudged elastic band (CI-NEB) method.[2] Eight images between the initial state (IS) and final state (FS) were used for the CI-NEB computations. The solvated proton was modelled by $H_5O_2^+$ near the reaction intermediates, following the recent experimental[3] and theoretical[4-5] studies. A linearized Poisson–Boltzmann implicit solvation model was used to neutralize the nonzero charge in the simulation, as implemented in VASPsol.[6] We employed a dielectric constant of 78.5 for water and a Debye length of 3.04 Å to simulate 1 mol of electrolyte solution of monovalent cations.

Surface Models

For models of Ru-NC_2 and Ru-N_3, we chose 6×6 supercell of graphene with 3×3×1 k-mesh, whereas 2×2 supercell of C_3N_4 and C_2N with 3×3×1 k-mesh were adopted in B-C_3N_4 and Mo-C_2N optimizations. For Ru-ZrO_2 model, 2×2 supercell of ZrO_2(111) surface with four ZrO_2 unit layers (containing 192 atoms) were used. Structural relaxations were performed by using 3×3×1 k-mesh, and top two ZrO_2 unit layers are fully relaxed while the bottom two layers are fixed during the geometry optimizations. The Mo-GDY was constructed by 1×1 unit cell since the effects of cell size on the adsorption energy are within 0.01 eV after a careful test.

DFT vs. DFT+U

The inclusion of the Hubbard-U term, or using the DFT+U approach, can give more accurate results for the systems with highly localized orbitals. However, the DFT+U approach also suffers from a strong (linear) dependence of the energetics on the choice of the value of the parameter U, and on the choice of the localized projector functions that enter the definition of the U-dependent energy term. For example, the reduction energy (ΔH) of $CeO_2 \rightarrow Ce_2O_3$ process can vary between −5.1 (U = 0 eV) and −1.9 eV (U = 5.0 eV) using the DFT+U method,[7] while the GGA-PBE value of −4.18 eV is in good agreement with the experimental measurements (−3.57 to −4.03 eV).

On the other hand, the U-value is usually chosen based on its accuracy in reproducing the electronic structures (i.e., experimental band gap) of the bulk materials. However, to simulate catalysts, it is better to choose *U* to fit the energy of the oxidation-reduction, since catalysts is controlled by energy difference.[8-9] Our specific case in this work, namely the NRR on BAC surfaces, involves complex surface–adsorbate interactions, thus, using the bulk properties-based *U* values in a locally changing surface environment may not describe reaction energetics correctly.[10-11]

Note that the results based on the GGA-PBE (the method used in this work) showed very good high performance in understanding the reaction mechanisms and activity trends observed in experiments.[4, 12]

To evaluate the accuracy of PBE results, we have investigated the NRR pathways on the Ti_2-Pc surface, one of the high-performance catalysts screened out in this work, by PBE+U method in which the previously validated *U* value of 2.58 eV was employed for Ti.[13] The computed theoretical limiting potential as well as the potential-liming step obtained by PBE+U are in good agreement with the PBE results (**Figure S16a**). Moreover, both total states and the 3d-oribital of Ti only differ slightly when *U*

is included (**Figure S16b, c**). Thus. PBE provides us an effective tool to qualitatively describe the NRR activity.

Due to the above reasons, we did not use DFT+U to consider the effect of the highly localized orbitals of the metal atoms in this work.

Table S1. Summary of structural parameters (lattice length a and b, angle γ and distance between two metal atoms) for 30 homonuclear M_2-Pc nanosheets, and the bond lengths of metal atoms in their bulk phase (D_{m-m}).

Metal	a (Å)	b (Å)	γ (degree)	d_{m-m} (Å)	D_{m-m} (Å)
Al	14.86	14.91	75.05	2.72	2.85
Sc	14.81	14.88	75.07	2.96	3.22
Ti	14.80	14.86	75.07	2.66	2.98
V	14.85	14.87	75.02	2.53	2.58
Cr	14.91	14.92	75.01	2.50	2.46
Mn	14.85	14.87	75.02	2.35	2.47
Fe	14.80	14.82	75.02	2.30	2.43
Co	14.79	14.81	75.02	2.36	2.48
Ni	14.85	14.88	75.04	2.73	2.49
Cu	14.84	14.89	75.04	2.73	2.57
Zn	14.81	14.88	75.08	2.73	2.97
Ga	14.90	14.96	75.06	2.78	2.77
Y	14.77	14.84	75.07	3.25	3.55
Zr	14.81	14.87	75.07	2.87	3.19
Nb	14.80	14.83	75.03	2.59	2.88
Mo	14.85	14.86	75.02	2.47	2.74
Ru	14.89	14.90	75.01	2.40	2.66
Rh	14.91	14.92	75.02	2.47	2.72
Pd	14.86	14.92	75.07	2.83	2.80
Ag	14.86	14.91	75.04	2.74	2.94
Sn	14.73	14.81	75.09	3.39	2.88
Hf	14.81	14.88	75.08	2.95	3.13
Ta	14.79	14.84	75.05	2.66	2.88
W	14.85	14.87	75.02	2.50	2.75
Re	14.88	14.89	75.01	2.38	2.75
Os	14.89	14.90	75.02	2.41	2.70
Ir	14.92	14.94	75.02	2.49	2.74
Pt	14.92	14.97	75.05	2.88	2.81
Au	14.90	14.94	75.04	2.81	2.95
Bi	14.77	14.85	75.08	3.41	3.11

Table S2. Computed cohesive energy ($E_c^{calc.}$), formation energy ($\mathbf{E}_f$) and dissolution potential ($\mathbf{U}_{diss}$) of metals, total energy of metal atoms in their bulk phase ($\mathbf{E}_M$) and number of transferred electrons (N_e) during the dissolution. For comparison, the experimental cohesive energy ($E_c^{exp.}$) and standard dissolution potential (U_{diss}°) of metal atoms are also listed.

Metal	$E_c^{exp.}$ (eV)	$E_c^{calc.}$ (eV)	N_e	U_{diss}° (V)	E_M (eV)	E_f (eV)	U_{diss} (V)
Al	-3.39	-3.55	3	-1.66	-3.75	-5.06	0.03
Sc	-3.90	-4.25	3	-2.08	-6.34	-5.13	-0.37
Ti	-4.85	-5.85	2	-1.63	-7.90	-4.09	0.42
V	-5.31	-5.59	2	-1.18	-9.09	-3.57	0.61
Cr	-4.10	-4.15	2	-0.91	-9.64	-3.53	0.85
Mn	-2.92	-4.02	2	-1.19	-9.16	-3.74	0.69
Fe	-4.28	-5.49	2	-0.45	-8.46	-3.32	1.21
Co	-4.39	-5.63	2	-0.28	-7.11	-3.18	1.31
Ni	-4.44	-5.39	2	-0.26	-5.78	-3.09	1.29
Cu	-3.49	-3.86	2	0.34	-4.10	-1.74	1.21
Zn	-135	-1.11	2	-0.76	-1.27	-2.09	0.28
Ga	-2.81	-2.85	3	-0.55	-3.04	-2.61	0.32
Y	-4.37	-4.19	3	-2.37	-6.47	-4.75	-0.79
Zr	-6.25	-6.59	4	-1.45	-8.55	-3.79	-0.50
Nb	-7.57	-7.65	3	-1.10	-10.11	-2.83	-0.16
Mo	-6.82	-6.27	3	-0.2	-10.86	-2.51	0.64
Ru	-6.74	-6.74	2	0.46	-9.28	-2.26	1.58
Rh	-5.75	-6.15	2	0.60	-7.36	-2.53	1.86
Pd	-3.89	-3.72	2	0.95	-5.18	-2.07	1.99
Ag	-2.95	-2.50	1	0.80	-2.83	-0.51	1.31
Sn	-3.14	-3.38	2	-0.14	-4.01	-1.63	0.66
Hf	-6.44	-6.48	4	-1.55	-9.95	-4.04	-0.54
Ta	-8.10	-8.41	3	-0.6	-11.86	-2.77	0.32
W	-8.90	-8.42	3	0.1	-12.96	-2.10	0.80
Re	-8.03	-7.83	3	0.3	-12.44	-2.26	1.05
Os	-8.17	-8.50	8	0.84	-11.22	-2.21	1.11
Ir	-6.94	-7.75	3	1.16	-8.86	-2.48	1.98
Pt	-5.84	-5.58	2	1.18	-6.06	-2.53	2.45
Au	-3.81	-3.62	3	1.50	-3.90	-0.36	1.62
Bi	-2.18	-2.57	1	0.5	-3.90	-1.33	1.83

Table S3. Computed vibrational frequencies, zero-point energies and entropy of reaction intermediates on Ti_2-Pc.

Reaction Intermediates	Vibrational Frequencies (cm^{-1})						ZPE (eV)	TS (eV)
N_2*	1801.92	521.36	379.90	319.32	229.07	138.30	0.21	0.10
N_2H*	3360.11 268.39	1352.76 220.66	1189.10 127.50	486.29	456.31	361.14	0.48	0.12
NHNH*	3374.50 617.74	3325.34 493.36	1410.24 439.56	1211.19 253.77	1001.87 246.05	811.70 121.26	0.82	0.11
NNH_2*	3421.55 622.94	3306.74 563.63	1591.23 378.41	1194.13 263.70	1130.79 235.40	892.50 107.25	0.85	0.12
$NHNH_2$*	3438.49 1132.24 168.88	3357.14 950.74 135.66	3292.75 585.08 119.34	1581.55 517.50	1341.94 346.85	1225.47 260.87	1.14	0.16
NH_2NH_2*	3439.53 1377.11 475.89	3421.24 1244.54 346.99	3335.87 1107.68 285.23	3324.16 1106.33 193.59	1597.50 947.05 132.45	1586.53 577.23 103.58	1.53	0.16
NH*-NH_3*	3505.30 1262.29 349.32	3502.95 807.83 283.52	3426.12 750.31 206.77	2744.31 633.57 165.26	1594.33 499.98 155.60	1577.44 373.98 141.93	1.36	0.20
NH*	3354.29	682.80	645.54	587.37	360.44	245.32	0.36	0.05
NH_2*	3500.04 479.72	3410.74 241.56	1503.77 196.50	706.59	675.79	573.92	0.70	0.08
NH_3*	3499.82 571.51	3480.49 559.86	3379.68 342.75	1614.21 142.30	1606.08 113.47	1201.42 84.93	1.03	0.16
H*	1238.61	903.10	708.10				0.18	0.01

Table S4. Computed vibrational frequencies, zero-point energies and entropy of reaction intermediates on V_2-Pc.

Reaction Intermediates	Vibrational Frequencies (cm^{-1})						ZPE (eV)	TS (eV)
N_2*	1754.85	497.57	348.59	325.64	209.18	143.72	0.20	0.10
N_2H*	3414.15 263.33	1258.57 213.83	1155.65 151.35	534.00	494.87	400.65	0.49	0.11
NHNH*	3404.47 546.55	3386.74 361.28	1380.18 341.42	1208.85 328.88	1155.60 253.46	550.67 159.72	0.81	0.12
NNH_2*	3385.80 583.71	3318.38 562.69	1575.35 373.84	1153.65 245.52	1139.05 208.59	883.71 96.19	0.84	0.13
$NHNH_2$*	3430.43 1116.10 204.38	3377.06 1004.02 186.80	3303.13 584.44 121.61	1575.14 557.65	1332.81 396.65	1210.15 264.85	1.16	0.15
NH_2NH_2*	3452.66 1378.07 516.93	3433.91 1204.13 382.31	3334.03 1104.06 345.97	3322.34 1093.03 177.73	1600.66 981.32 169.26	1584.46 555.10 106.29	1.53	0.15
NH*-NH_3*	3524.16 1197.17 375.42	3498.51 852.43 191.44	3484.19 637.82 181.28	3371.16 626.27 166.47	1602.94 427.45 130.77	1583.45 385.06 85.55	1.38	0.18
NH*	3454.31	737.44	729.33	406.19	356.50	284.65	0.37	0.05
NH_2*	3514.10 549.50	3427.76 296.36	1510.15 200.88	724.87	720.80	648.60	0.72	0.07
NH_3*	3491.29 610.16	3487.94 597.19	3384.26 364.52	1610.69 133.07	1604.13 131.90	1192.04 86.55	1.03	0.15
H*	1412.18	1010.13	753.12				0.20	0.00(4)

Table S5. Computed vibrational frequencies, zero-point energies and entropy of reaction intermediates on Re_2-Pc.

Reaction Intermediates	Vibrational Frequencies (cm^{-1})						ZPE (eV)	TS (eV)
N_2*	2125.26	427.50	391.76	377.77	126.99	103.33	0.22	0.12
N_2H*	3170.20 333.30	1693.95 127.67	1130.08 69.04	548.36	430.25	335.84	0.48	0.09
NNH_2*	3518.00 615.80	3105.84 404.34	1538.49 378.70	1332.02 303.79	1220.34 176.66	634.74 95.40	0.83	0.13
NHNH*	3418.59 637.22	3415.53 524.96	1338.43 504.92	1204.72 440.12	1001.09 335.35	699.59 218.27	0.85	0.08
N*	1053.89	241.35	233.34				0.09	0.05
NH*	3314.77	981.15	897.08	613.62	322.49	276.44	0.40	0.05
NH_2*	3527.38 583.91	3428.60 366.84	1511.30 276.88	814.66	788.65	781.83	0.75	0.05
NH_3*	3446.66 708.60	3442.14 703.06	3326.70 400.19	1601.18 143.68	1587.03 94.32	1237.39 25.48	1.03	0.10
$NHNH_2$*	3432.31 1168.38 235.85	3416.38 848.53 94.20	3336.60 631.24 27.74	1620.43 502.18	1427.00 342.30	1236.44 319.92	1.16	0.18
NH_2NH_2*	3418.75 1449.65 439.59	3398.70 1242.32 252.38	3346.02 1123.67 224.57	3188.51 1106.58 92.03	1638.18 917.07 74.37	1587.60 671.05 61.53	1.39	0.22
H*	2146.73	624.88	359.82				0.19	0.02

Table S6. Summary of NH_3* adsorption energies ($\Delta G_{NH_3^*}$) on 31 BACs which were screened out by activity analysis. The $\Delta G_{NH_3^*}$ refers to the free energy of NH_3 in free gas.

Dimers	ZPE	TS	$\Delta G_{NH_3^*}$
Ti_2	1.03	0.16	-1.06
V_2	1.03	0.15	-0.90
Re_2	1.03	0.10	-0.43
TiV	1.02	0.11	-0.57
TiCu	1.03	0.16	-1.15
TiZn	1.03	0.16	-1.22
TiAl	1.02	0.17	-1.11
TiGa	1.02	0.17	-1.17
TiAg	1.03	0.16	-1.15
TiTa	1.02	0.16	-1.06
TiW	1.02	0.16	-1.03
TiAu	1.02	0.12	-1.14
VCr	1.03	0.15	-1.05
VZn	1.03	0.17	-1.29
VMo	1.04	0.14	-1.16
VSn	1.03	0.15	-0.98
VTa	1.03	0.11	-1.48
VW	1.04	0.14	-1.10
VPt	1.03	0.16	-0.97
TaCr	1.03	0.11	-1.23
TaMn	1.03	0.16	-1.32
TaFe	1.04	0.15	-1.32
TaCo	1.03	0.18	-1.41
TaAl	1.03	0.18	-0.78
TaMo	1.03	0.16	-1.26
TaRu	1.03	0.16	-1.29
TaRh	1.03	0.17	-1.49
TaW	0.96	0.06	-1.38
TaOs	1.04	0.14	-1.38
TaIr	1.03	0.17	-1.50
TaBi	1.03	0.16	-0.68

Table S7. Computed vibrational frequencies, zero-point energies and entropy of key intermediates on B-C_3N_4, Mo-C_2N, Mo-GDY, B_4C(110), Ru-N_3, Ru-NC_2,Ru-ZrO_2 and Mn_2-C_2N surfaces. The results of B-C_3N_4 reported earlier[14] are also provided for comparison, which denoted as B-$C_3N_4^{\#}$.

Catalysts	Reaction Intermediates	Vibrational Frequencies (cm^{-1})						ZPE (eV)	TS (eV)
B-C_3N_4	**H***	2646.63	1006.23	629.81				0.27	0.01
	End-on N_2*	2090.30	579.00	435.46	385.00	126.96	71.85	0.23	0.12
	N_2H*	3136.12 266.52	1633.49 90.725	1311.44 62.71	624.40	609.80	281.10	0.50	0.16
B-$C_3N_4^{\#}$	**End-on N_2***	2088.78	577.56	439.11	397.28	128.77	101.88	0.23	0.11
	N_2H*	3139.78 263.83	1750.39 129.57	1312.97 62.90	629.86	556.59	360.05	0.50	0.14
Mo-C_2N	**H***	1938.94	520.63	452.41				0.18	0.02
	End-on N_2*	2091.80	415.78	397.78	372.66	75.18	69.14	0.21	0.14
	N_2H*	3257.711 301.90	1640.45 93.71	1111.48 81.01	532.51	446.09	364.94	0.49	0.15
Mo-GDY	**H***	1767.29	559.07	431.40				0.17	0.018
	End-on N_2*	1776.28	585.09	349.80	214.40	126.55	88.44	0.19	0.13
	N_2H*	3219.27 153.45	1386.51 103.28	1212.38 61.43	613.05	487.04	357.66	0.47	0.16
Ru-N_3	**H***	1834.10	628.34	594.70				0.19	0.01
	End-on N_2*	2143.98	468.21	433.34	389.14	83.01	66.43	0.22	0.14
	N_2H*	3107.60 246.48	1629.35 81.24	1199.17 45.06	600.01	531.74	416.08	0.48	0.10
Ru-NC_2	**H***	1796.42	595.64	505.45				0.18	0.01
	End-on N_2*	2174.28	365.53	332.46	276.54	46.44	37.12	0.20	0.11
	N_2H*	3051.56 296.78	1632.86 51.67	1231.60 47.56	629.79	468.57	329.82	0.48	0.18
Ru-ZrO_2	**H***	1691.64	666.81	424.34				0.17	0.02
	End-on N_2*	2175.70	441.20	406.13	379.07	71.09	43.41	0.22	0.16
	N_2H*	3103.51 287.07	1732.51 94.17	1117.79 73.88	490.60	448.36	365.58	0.48	0.15

Table S8. Summary of adsorption energy of N_2H^* ($\Delta E_{N_2H^*}, eV$), limiting potential ($U_L, V\ vs. SHE$), potential limiting step (PDS), and Gibbs free energies of N_2^* ($\Delta G_{N_2^*}, eV$) and H* ($\Delta G_{H^*}, eV$) on 37 heteronuclear MM'-Pc. Systems with U_L more negative than that of stepped Ru(0001) were highlighted by red color.

Dimers	$\Delta E_{N_2H^*}$	U_L	PDS	$\Delta G_{N_2^*}$	ΔG_{H^*}
TiV	-1.27	-0.74	$NH_2^*\rightarrow NH_3^*$	-0.50	-0.33
TiCu	-0.55	-0.53	$N_2^*\rightarrow N_2H^*$	-0.15	-0.31
TiZn	-0.34	-0.58	$N_2^*\rightarrow N_2H^*$	0.07	-0.05
TiAl	-0.75	-0.45	$N_2^*\rightarrow N_2H^*$	-0.27	-0.52
TiGa	-0.78	-0.45	$N_2^*\rightarrow N_2H^*$	-0.31	-0.51
TiAg	-0.75	-0.49	$N_2^*\rightarrow N_2H^*$	-0.31	-0.47
TiTa	-0.93	-0.74	$NH_2^*\rightarrow NH_3^*$	-0.51	-0.74
TiW	-0.42	-0.52	$N_2^*\rightarrow N_2H^*$	0.01	-0.02
TiAu	-0.77	-0.48	$N_2^*\rightarrow N_2H^*$	-0.32	-0.49
VCr	-0.52	-0.85	$N_2^*\rightarrow N_2H^*$	-0.44	0.34
VZn	-0.42	-0.55	$N_2^*\rightarrow N_2H^*$	-0.03	-0.27
VMo	-1.44	-0.32	$NH_2^*\rightarrow NH_3^*$	-0.39	-0.66
VSn	-0.52	-0.78	$N_2^*\rightarrow N_2H^*$	-0.37	-0.01
VTa	-2.22	-0.47	$NH_2^*\rightarrow NH_3^*$	-1.19	-1.17
VW	-1.50	-0.42	$NH_2^*\rightarrow NH_3^*$	-0.37	-1.02
VPt	-0.55	-0.76	$N_2^*\rightarrow N_2H^*$	-0.40	-0.08
TaCr	-1.22	-0.58	$NHNH^*\rightarrow NHNH_2^*$	-0.17	-1.10
TaMn	-1.14	-0.71	$NH_2^*\rightarrow NH_3^*$	-0.14	-1.10
TaFe	-0.93	-0.78	$NH_2^*\rightarrow NH_3^*$	-0.57	-1.14
TaCo	-0.92	-0.67	$NH_2^*\rightarrow NH_3^*$	-0.66	-1.10
TaNi	-1.13	-1.21	$NH_2^*\rightarrow NH_3^*$	-0.28	\
TaCu	-1.15	-1.14	$NH_2^*\rightarrow NH_3^*$	-0.37	\
TaZn	-1.14	-1.09	$NH_2^*\rightarrow NH_3^*$	-0.33	\
TaAl	-1.16	-0.43	$NH_2^*\rightarrow NH_3^*$	-0.65	-1.08
TaGa	-1.14	-1.05	$NH_2^*\rightarrow NH_3^*$	-0.72	\
TaMo	-0.66	-0.89	$N_2^*\rightarrow N_2H^*$	-0.66	-0.61
TaRu	-0.70	-0.64	$N_2^*\rightarrow N_2H^*$	-0.47	-0.82
TaRh	-0.87	-0.73	$N_2^*\rightarrow N_2H^*$	-0.70	-0.98
TaPd	-1.08	-1.20	$NH_2^*\rightarrow NH_3^*$	-0.24	\
TaAg	-1.14	-1.03	$NH_2^*\rightarrow NH_3^*$	-0.64	\
TaSn	-1.09	-1.07	$NH_2^*\rightarrow NH_3^*$	-0.30	\
TaW	-1.51	-0.86	$NH_2^*\rightarrow NH_3^*$	-0.79	-1.09
TaOs	-0.88	-0.67	$N_2^*\rightarrow N_2H^*$	-0.66	-1.00
TaIr	-0.86	-0.75	$N_2^*\rightarrow N_2H^*$	-0.70	-0.98
TaPt	-1.09	-1.21	$NH_2^*\rightarrow NH_3^*$	-0.58	\
TaAu	-1.13	-1.08	$NH_2^*\rightarrow NH_3^*$	-0.73	\
TaBi	-0.48	-0.83	$NH_2^*\rightarrow NH_3^*$	0.34	-0.63

Table S9. Computed total energies (E) and thermodynamic quantities, in eV, for the gas phase N_2, H_2, NH_3 species. (T = 298.15 K, P = 1 bar), and free H_2O at the 298.15 K, 0.035 bar. In comparison, the experimental entropies (TS_{exp}) of the gas phase N_2, H_2, NH_3 and H_2O are also shown, which are from NIST standard reference database (https://doi.org/10.18434/T4D303).

Species	**E**	**TS_{t+r+v}**	**ZPE**	**G**	**TS_{exp}**
N_2 (g)	-16.61	0.59	0.15	-17.05	0.59
H_2 (g)	-6.76	0.40	0.27	-6.89	0.41
NH_3 (g)	-19.52	0.60	0.91	-19.20	0.60
H2O (l)	-14.22	0.67	0.57	-14.33	0.67

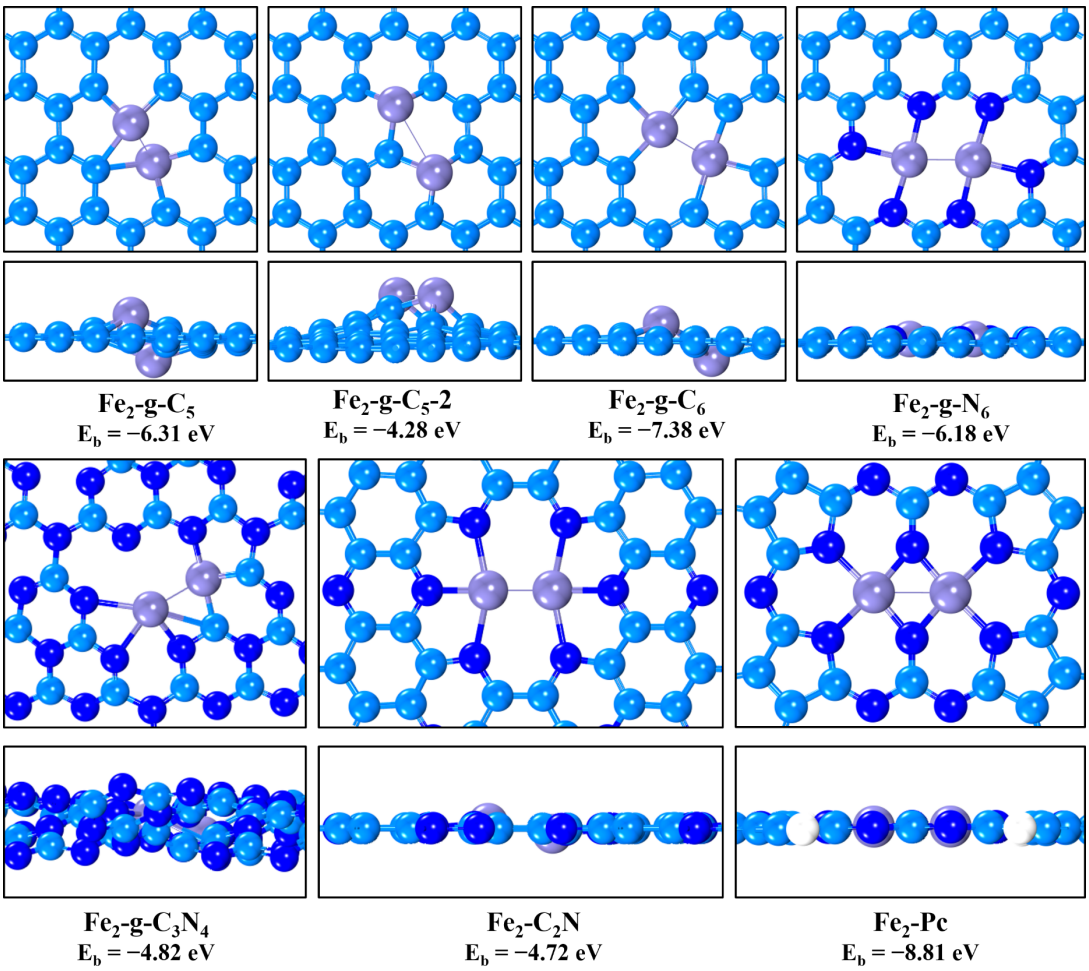

Figure S1. Optimized configurations and binding energies of Fe dimers anchored on defective and nitrogen-doped graphene, defective C_3N_4, C_2N, and rectangular-shaped expanded phthalocyanine.

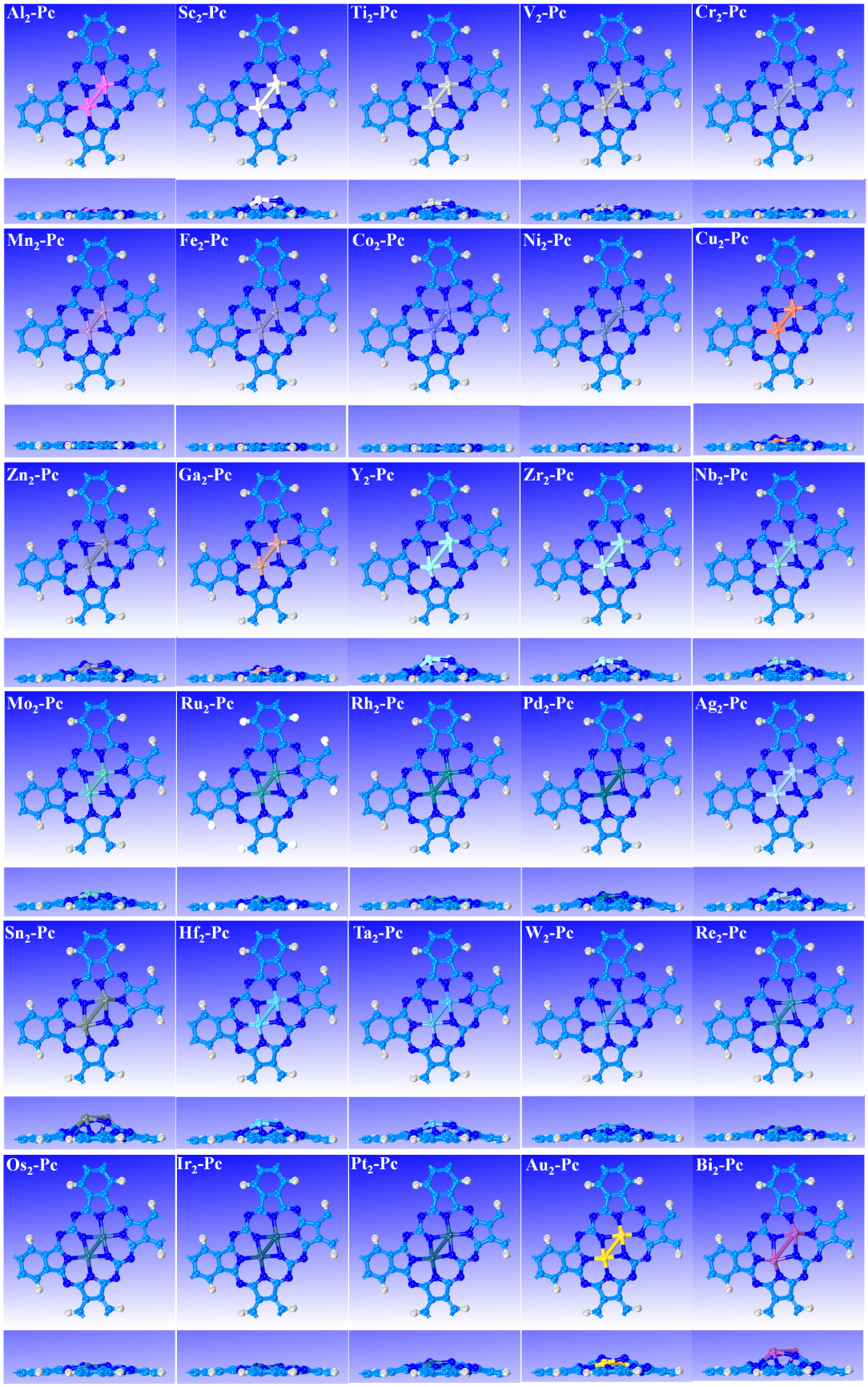

Figure S2. Optimized structures of M_2-Pc nanosheet.

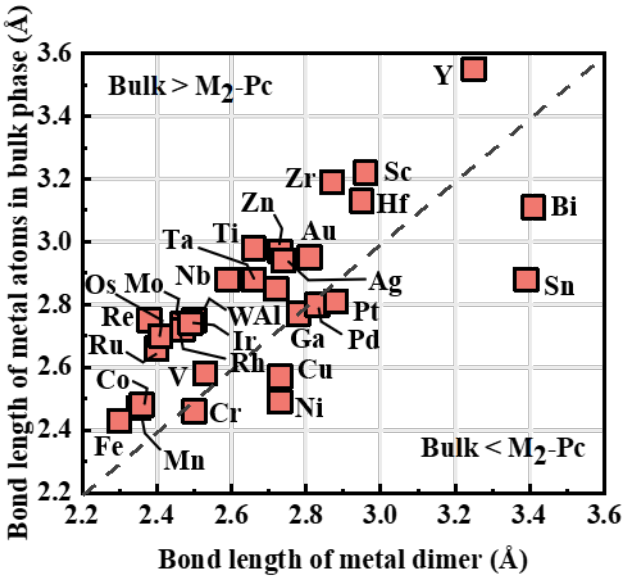

Figure S3. Computed bond lengths of metal dimers in M_2-Pc versus the bond lengths in its bulk phases.

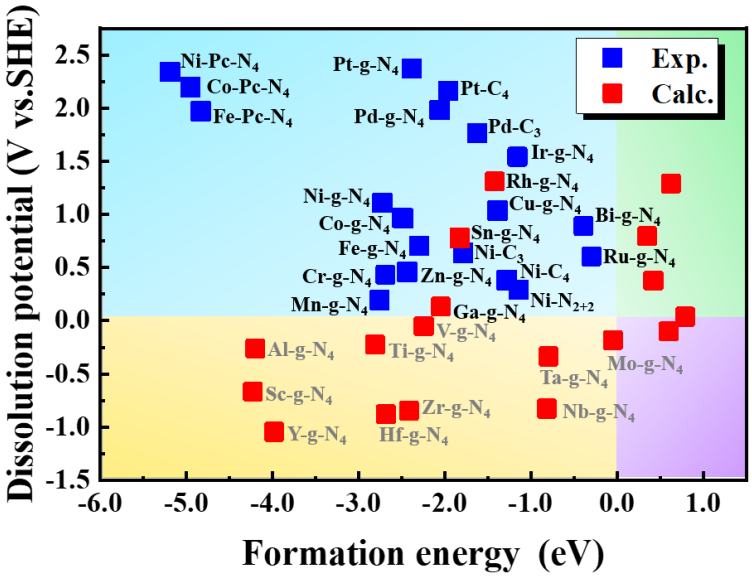

Figure S4. Variations of formation energy (E_f) and dissolution potential (U_{diss}) of metal atoms on phthalocyanine (Pc-N_4), graphene (g-C_3 and g-C_4) and N-doped carbon materials (g-N_4). The experimentally reported SACs were highlighted by **blue**.

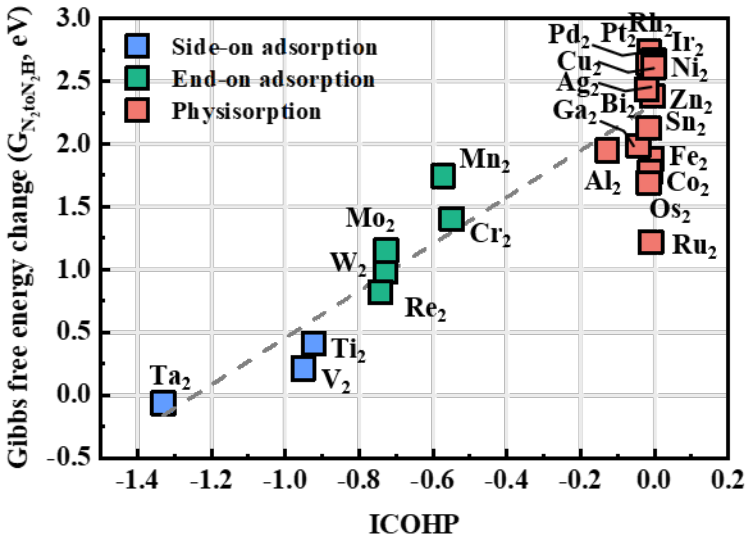

Figure S5. Calculated ICOHP versus the free energy change of the first elementary step for NRR.

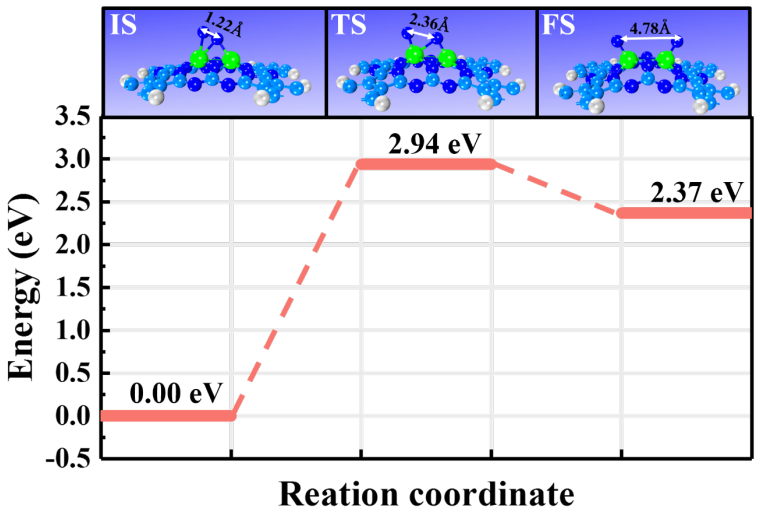

Figure S6. Reaction pathway of N_2 dissociation on Ta_2-Pc surface. The optimized initial, transition and final states of N_2 on Ta_2-Pc are shown in insets.

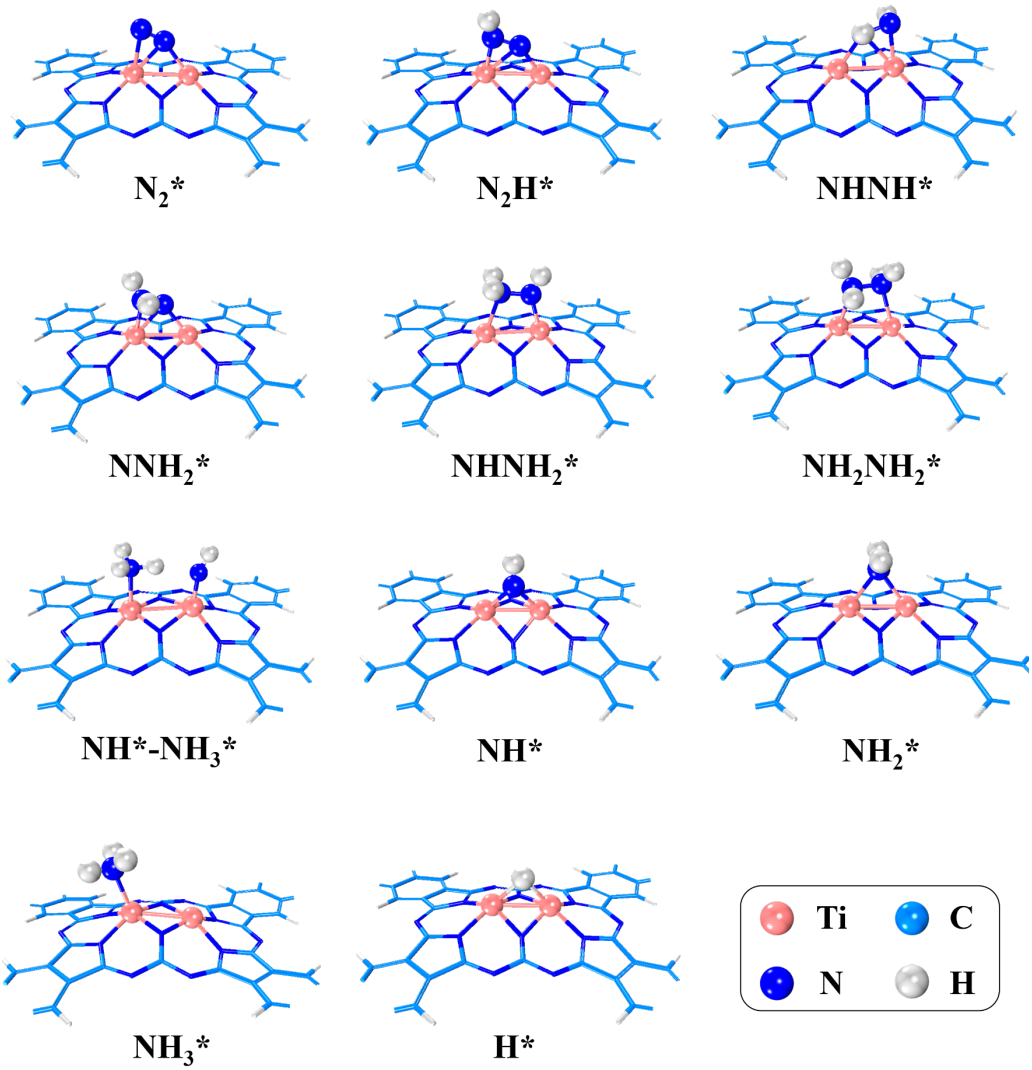

Figure S7. Optimized structures of reaction intermediate on Ti_2-Pc surface.

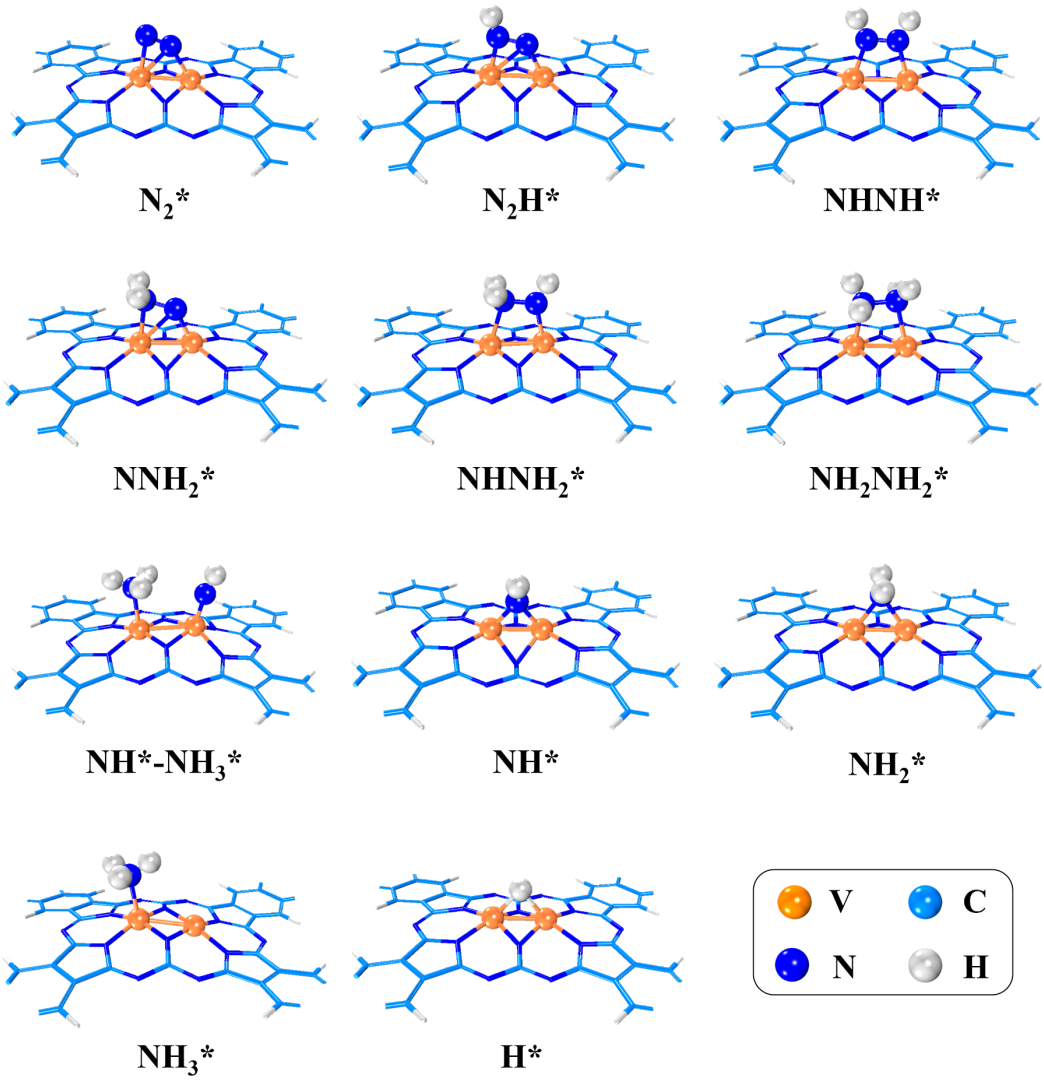

Figure S8. Optimized structures of reaction intermediate on V_2-Pc surface.

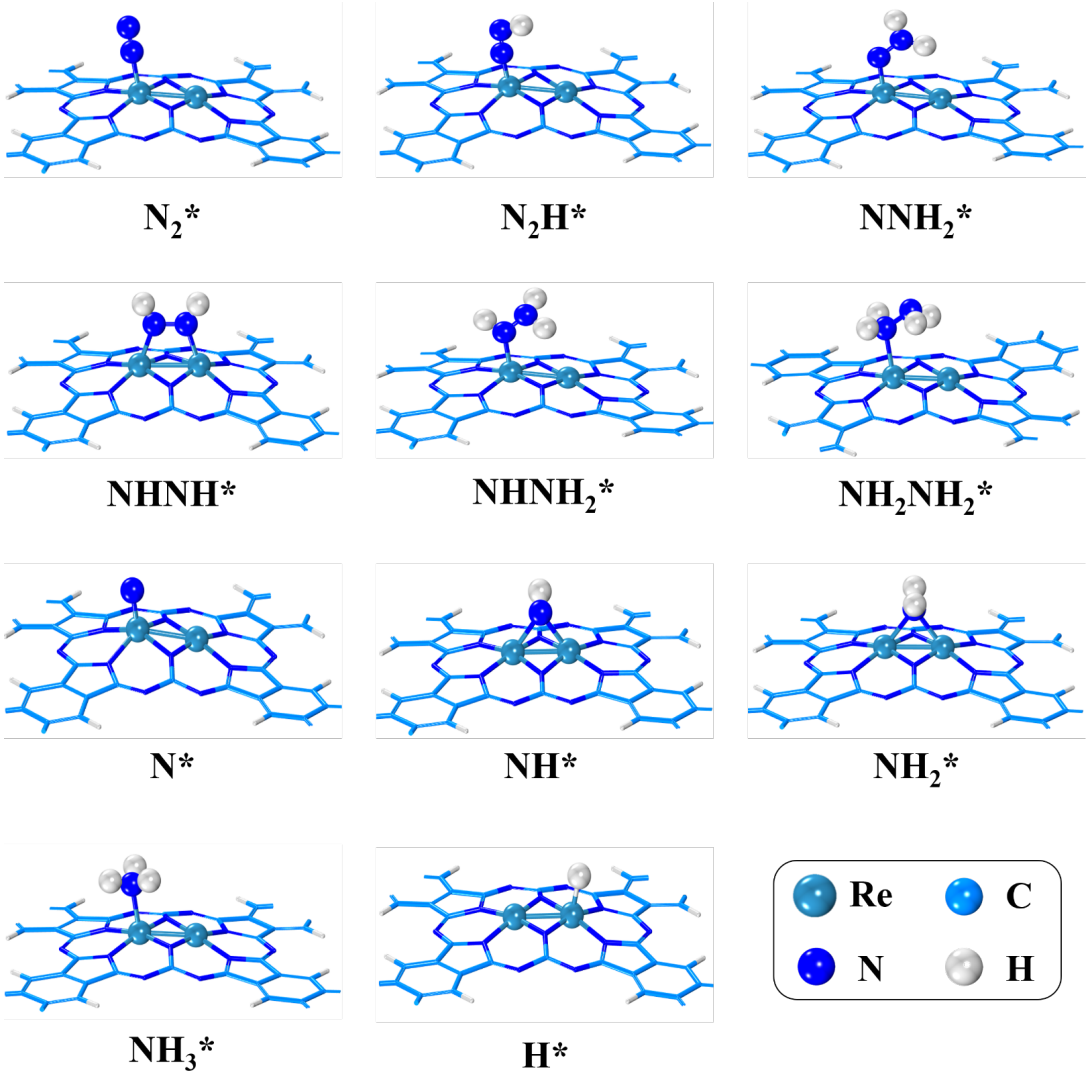

Figure S9. Optimized structures of reaction intermediate on Re_2-Pc surface.

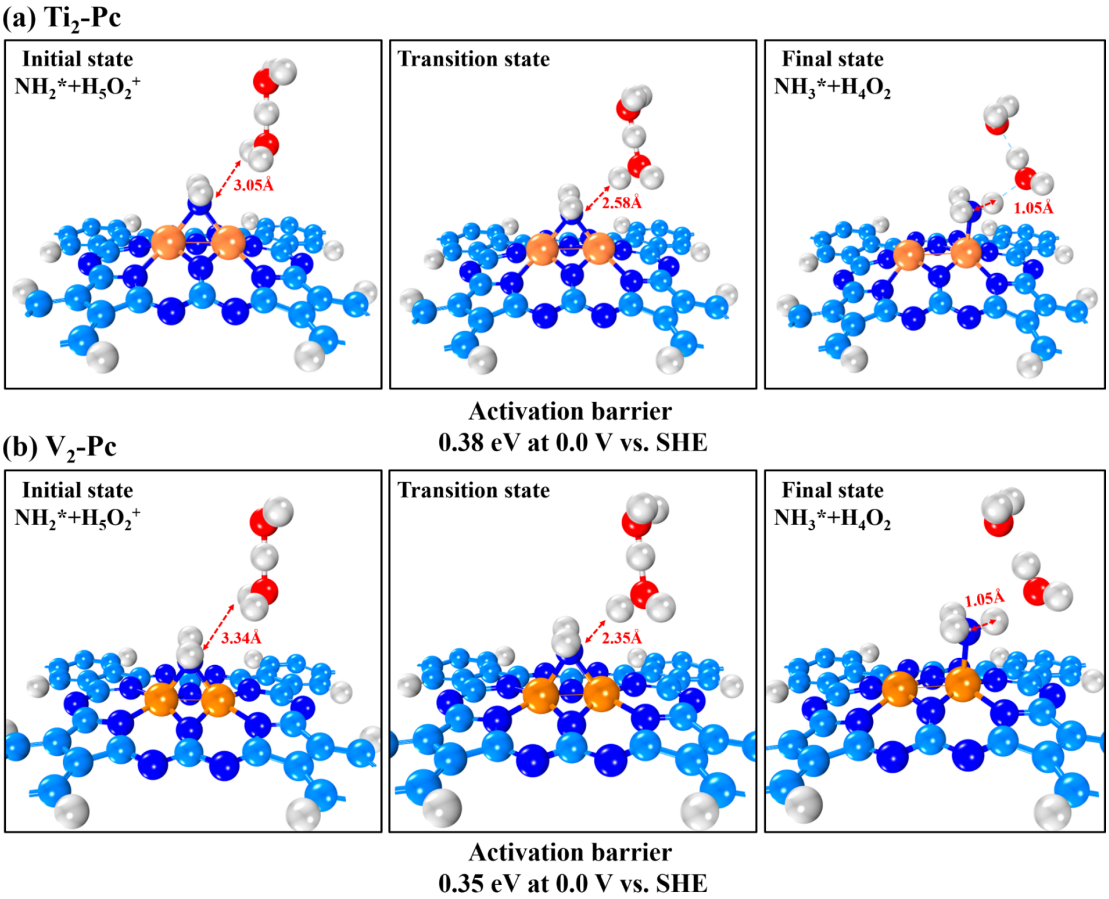

Figure S10. Optimized structures and related kinetic barriers of reduction of NH_2* to NH_3* on Ti_2-Pc and V_2-Pc surfaces.

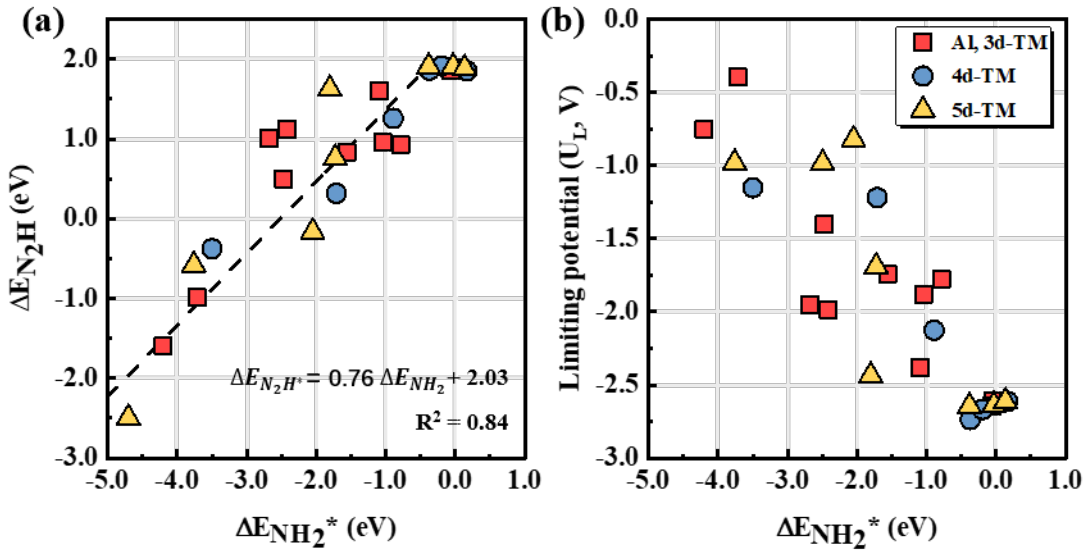

Figure S11. The correlation between the NH_2* adsorption energy ($\Delta E_{NH_2^*}$) and the adsorption energy of N_2H* ($\Delta E_{N_2H^*}$) (a) as well as the limiting potential (b) on 25 homonuclear BACs.

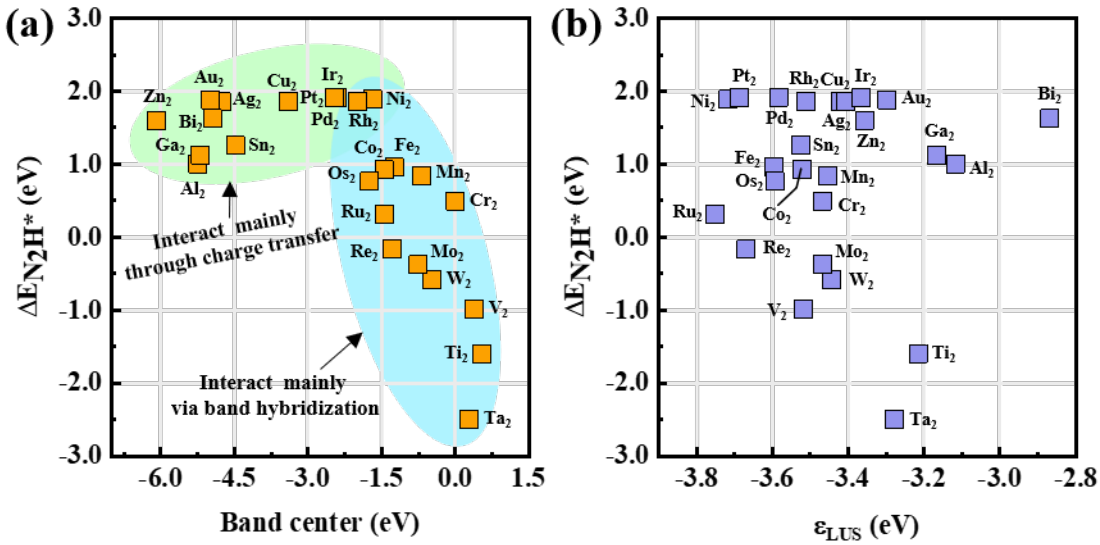

Figure S12. Correlations between the N_2H adsorption energy ($\Delta E_{N_2H^*}$) and the band center of adsorbed metal atoms (a), and the energy of lowest unoccupied state (ε_{LUS}) of 25 homonuclear BACs (b). The band center refers to the d-band center for transition metal, whereas refers to the p-band center for the main group elements (Al, Ga, Sn, and Bi).

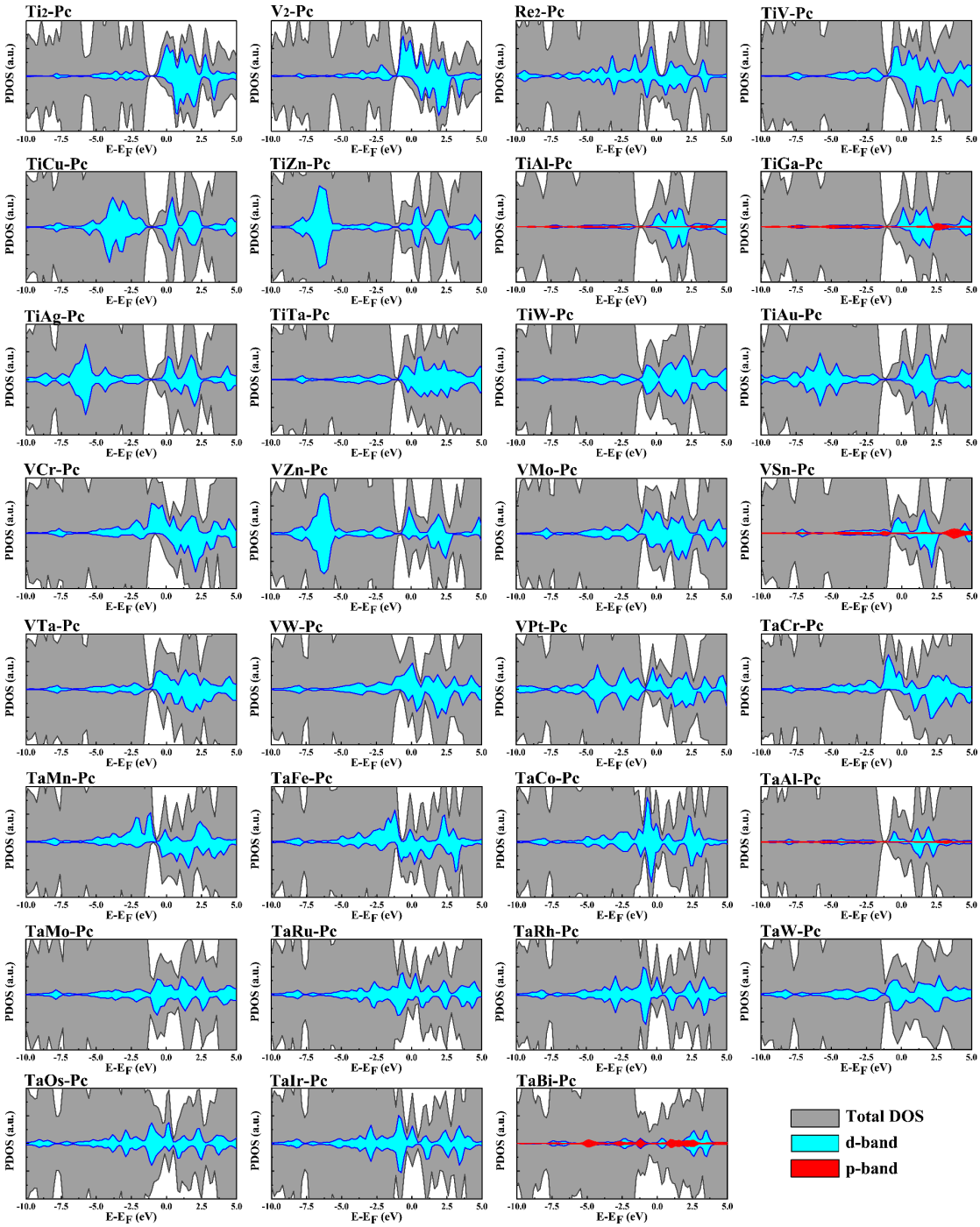

Figure S13. Computed partial density of states (PDOS) of 3 homonuclear and 28 heteronuclear MM'-Pc which predicted with less negative U_L with respect to the stepped Ru(0001). The Fermi level is set to be 0 V.

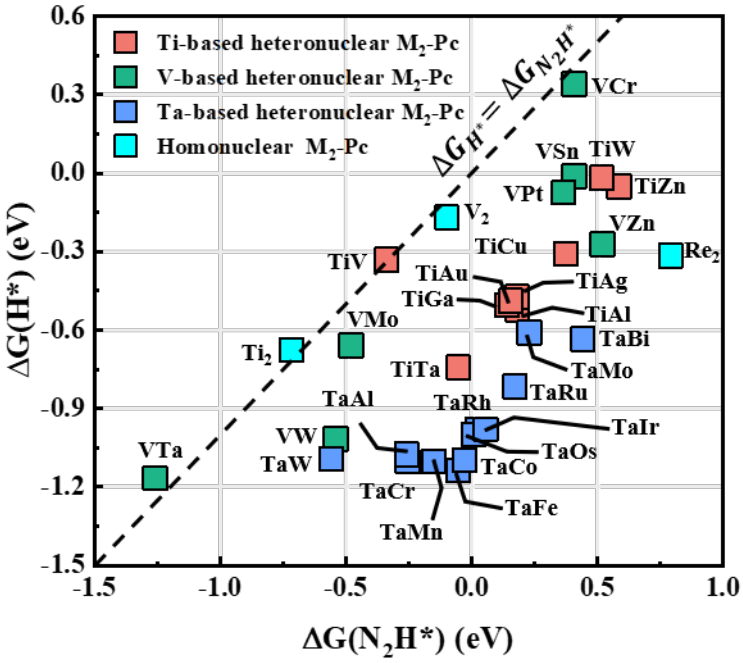

Figure S14. Relations between $\Delta G_{N_2H^*}$ and ΔG_{H^*} on 31 MM'-Pc systems which screened by activity analysis.

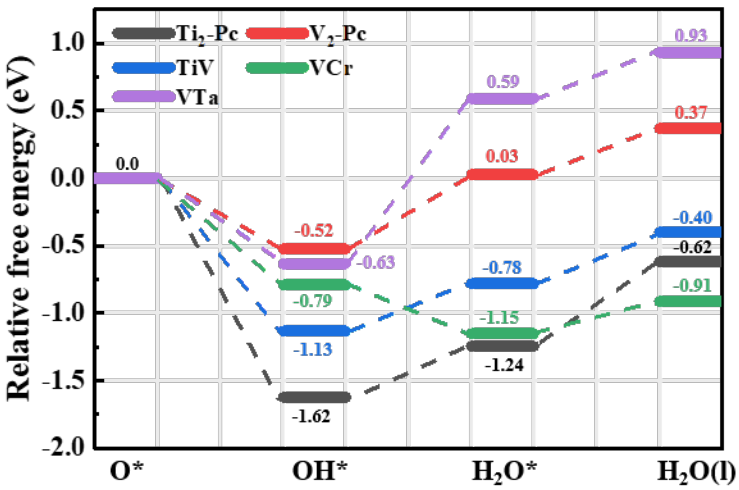

Figure S15. Relative free energy changes along the deoxidation/dehydroxylation process on the Ti_2-Pc, V_2-Pc, TiV-Pc, VCr-Pc, and VTa-Pc surfaces at the potential of U_L.

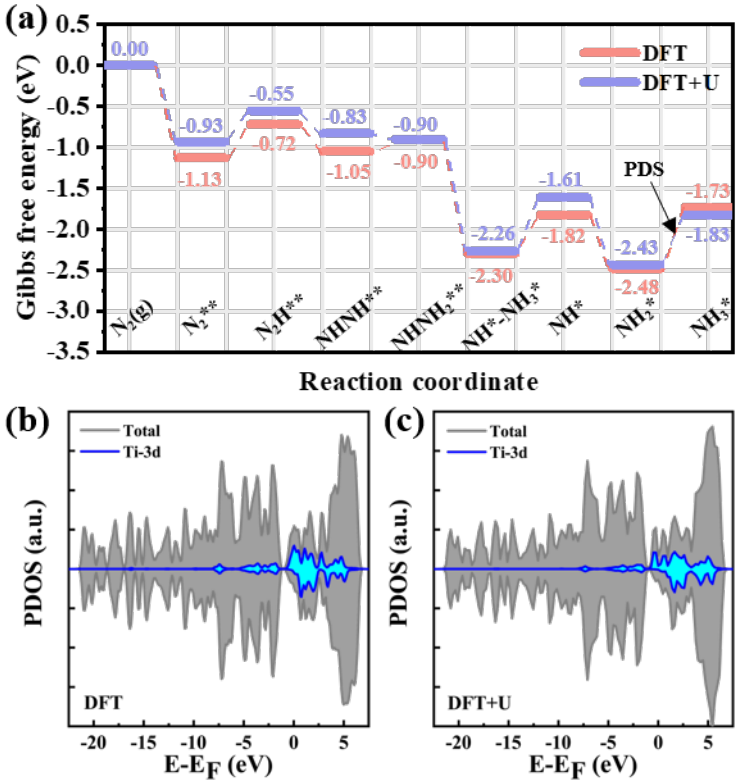

Figure S16. Comparison of nitrogen reduction reaction pathways on the Ti_2-Pc (a), and density of states of Ti_2-Pc (b, c) by using the DFT and DFT+U methods.

REFERENCES

1. Nørskov, J. K.; Rossmeisl, J.; Logadottir, A.; Lindqvist, L.; Kitchin, J. R.; Bligaard, T.; Jonsson, H. Origin of the Overpotential for Oxygen Reduction at A Fuel-Cell Cathode. *J. Phys. Chem. B* **2004,** *108*, 17886-17892.

2. Henkelman, G.; Uberuaga, B. P.; Jónsson, H. A Climbing Image Nudged Elastic Band Method for Finding Saddle Points and Minimum Energy Paths. *J. Chem. Phys.* **2000,** *113*, 9901-9904.

3. Stoyanov, E. S.; Stoyanova, I. V.; Reed, C. A. The Structure of the Hydrogen Ion (H_{aq}^+) in Water. *J. Am. Chem. Soc.* **2010,** *132*, 1484-1485.

4. Wang, Y.; Tang, Y.-J.; Zhou, K. Self-Adjusting Activity Induced by Intrinsic Reaction Intermediate in Fe–N–C Single-Atom Catalysts. *J. Am. Chem. Soc.* **2019,** *141*, 14115-14119.

5. Chang, K.; Zhang, H.; Chen, J. G.; Lu, Q.; Cheng, M. J. Constant Electrode Potential Quantum Mechanical Study of CO_2 Electrochemical Reduction Catalyzed by N-Doped Graphene. *ACS Catal.* **2019,** *9*, 8197-8207.

6. Mathew, K.; Sundararaman, R.; Letchworth-Weaver, K.; Arias, T. A.; Hennig, R. G. Implicit Solvation Model for Density-Functional Study of Nanocrystal Surfaces and Reaction Pathways. *J. Chem. Phys.* **2014,** *140*, 084106.

7. Huang, M.; Fabris, S. CO Adsorption and Oxidation on Ceria Surfaces from DFT+U Calculations. *J. Phys. Chem. C* **2008,** *112*, 8643-8648.

8. Tolba, S. A.; Gameel, K. M.; Ali, B. A.; Almossalami, H. A.; Allam, N. K. The DFT+ U: Approaches, Accuracy, and Applications. *Density Functional Calculations: Recent Progresses of Theory and Application.* InTech: London, 2018, 1. DOI: 10.5772/intechopen.72020

9. Hu, Z.; Metiu, H. Choice of U for DFT+U Calculations for Titanium Oxides. *J. Phys. Chem. C*

2011, *115*, 5841-5845.

10. Bhola, K.; Varghese, J. J.; Dapeng, L.; Liu, Y.; Mushrif, S. H. Influence of Hubbard U Parameter in Simulating Adsorption and Reactivity on CuO: Combined Theoretical and Experimental Study. *The J. Phys. Chem. C* **2017,** *121*, 21343-21353.

11. Fronzi, M.; Piccinin, S.; Delley, B.; Traversa, E.; Stampfl, C. Water Adsorption on the Stoichiometric and Reduced CeO_2(111) Surface: A First-Principles Investigation. *Phys. Chem. Chem. Phys.* **2009,** *11*, 9188-9199.

12. Zhang, Z.; Xiao, J.; Chen, X.-J.; Yu, S.; Yu, L.; Si, R.; Wang, Y.; Wang, S.; Meng, X.; Wang, Y.; Tian, Z.-Q.; Deng, D. Reaction Mechanisms of Well-Defined Metal–N_4 Sites in Electrocatalytic CO_2 Reduction. *Angew. Chem. Int. Ed.* **2018,** *57*, 16339-16342.

13. Xu, H.; Cheng, D.; Cao, D.; Zeng, X. C. A Universal Principle for A Rational Design of Single-Atom Electrocatalysts. *Nat. Catal.* **2018,** *1*, 339-348.

14. Ling, C.; Niu, X.; Li, Q.; Du, A.; Wang, J. Metal-Free Single Atom Catalyst for N_2 Fixation Driven by Visible Light. *J. Am. Chem. Soc.* **2018,** *140*, 14161-14168.